Work function, optical absorption, and second-harmonic generation from alkali-metal atoms adsorbed on metal surfaces

B. N. J. Persson
Institut für Festkörperforschung, Kernforschungsanlage Jülich, D-5170 Jülich, West Germany

L. H. Dubois
AT&T Bell Laboratories, Murray Hill, New Jersey 07974

(Received 11 July 1988; revised manuscript received 24 October 1988)

We consider the electronic properties of a low coverage of alkali-metal atoms adsorbed on a metal surface. We calculate the alkali-metal-induced changes in the work function, optical absorption, and second-harmonic generation within a simple but realistic model. The alkali-metal-induced peak typically observed at a few eV loss energy in inelastic electron scattering is explained as resulting from electronic transitions from the filled part of the *ns* resonance to the empty part of the same resonance and to the *np* resonance. We predict a strong alkali-metal-induced increase in the low-frequency lossy response of an alkali-metal-covered metal surface. This theoretical prediction is confirmed by new inelastic-electron-scattering data for the K/Cu(100) system. A strong increase in second-harmonic generation (SHG) is predicted at low alkali-metal concentration (laser photon energy $\hbar\omega \simeq 1.16$ eV). The dependence of the SHG signal on the coverage (at low coverage) and on the incident photon energy is in rough agreement with experimental data. Finally, we discuss the temperature dependence of the work function and of the local fluctuating electric field which exists in the adsorbate system. Experimental results for the temperature dependence of the work function for the K/Cu(100) system are presented and are found to be in good agreement with the theoretical predictions.

I. INTRODUCTION

Because of their great technological relevance, alkali-metal atoms adsorbed on both noble- and transition-metal surfaces have been well-studied chemisorption systems.[1] For example, the strong decrease in the work function which is induced by alkali-metal adsorption is used in high electron emission cathodes. Another important application is in catalysis where a small concentration of adsorbed alkali-metal atoms is found to enhance the reaction rate or selectivity of many chemical reactions. A wide variety of surface sensitive techniques have been used to study these systems including work-function measurements, electron-energy-loss spectroscopy (EELS),[2] inverse photoemission,[3] second-harmonic generation (SHG),[4,5] and metastable helium deexcitation spectroscopy.[6]

In this work we will use a simple but realistic model[7] to calculate the variation of the work function and the EEL and SHG spectra with alkali-metal coverage. The work function is determined by the static (zero-order) dipole moment, while the EEL and SHG signals are determined by the dynamical, first-order (in the external driving field) and second-order dipole moments, respectively. All these quantities are calculated using the same model, with model parameters chosen to reproduce the measured work-function data for K on Cu(100).

In Sec. II we define the model used in this work and in Sec. III we calculate the coverage-dependent work function. In Sec. IV we discuss the frequency-dependent polarizability associated with an ordered lattice of adsorbed alkali-metal atoms; the imaginary part of this polarizability determines the alkali-metal-induced EEL intensity. We predict a strong alkali-metal-induced increase of the low-frequency "lossy" response of an alkali-metal-covered metal surface. This theoretical prediction is confirmed by new inelastic-electron-scattering data for the K/Cu(100) system. In Sec. V we calculate the SHG spectra for an alkali-metal-covered metal surface, and discuss the experimental data of Song *et al.* Section VI is devoted to a study of temperature-dependent local fields which exist in alkali-metal adsorbate systems and which influence many of their properties. We predict that the work function of an alkali-metal-covered surface increases with increasing temperature. Work-function measurements on the K/Cu(100) system are in quantitative agreement with these theoretical predictions. Section VII contains a summary.

II. THE MODEL

The two most characteristic properties of alkali-metal atoms are their small ionization energy and huge static polarizability (see Table I). Both of these properties are crucial for the understanding of the static (e.g., work-function change) and dynamical (e.g., optical absorption or second-harmonic generation) properties of alkali-metal atoms adsorbed on transition- or noble-metal surfaces.

The static polarizability of the alkali-metal atoms is almost entirely due to the $ns \rightarrow np$ transition, where *ns* is the highest occupied *s* level (e.g., 3*s* in Na) and *np* the

TABLE I. The ionization energy I, the static polarizability $\alpha(0)$, the energy separation ΔE between the np and ns levels, and the transition dipole moment $e\lambda$.

	Na	K	Rb	Cs
I (eV)	5.14	4.3	4.2	3.9
$\alpha(0)$ (Å^3)	20	36	40	53
ΔE (eV)	2.1	1.6	1.5	1.4
λ (Å)	1.20	1.41	1.44	1.60

lowest unoccupied p level (e.g., $3p$ in Na). Hence, the low-frequency polarizability of an alkali-metal atom is accurately given by

$$\alpha=\lambda^2e^2\left[\frac{1}{\Delta E-\omega}+\frac{1}{\Delta E+\omega}\right]\rightarrow\frac{2\lambda^2e^2}{\Delta E}$$

as the frequency $\omega\rightarrow 0$. From the known separation $\Delta E=\varepsilon_p-\varepsilon_s$ between the np and ns levels and from the known static polarizability $\alpha(0)$ given in Table I one can derive the value for the parameter λ (see Table I).

Consider now an alkali-metal atom well outside a metal surface. The energy released on transferring an electron from the alkali-metal atom (ionization energy I) to the metal (work function ϕ) is $\phi-I$. Next, if the positively charged alkali-metal atom is brought to its equilibrium position on the surface, an energy $e^2/4d$ is released (assuming that the alkali-metal atom stays fully ionized and neglecting the work done against the repulsive part of the ion-metal interaction potential), where d is the separation between the center of the alkali-metal ion and the image reference plane of the metal. Hence, within this simple model, the alkali-metal binding energy is

$$E_B=\phi-I+e^2/4d\ .$$

Since for alkali-metal atoms $I\sim 4$–5 eV and for a typical transition metal $\phi\sim 4$ eV, one gets $E_B\approx 3$–4 eV if $d\approx 1$ Å as expected in most cases. This binding energy is slightly larger than that observed experimentally (typically $E_B=2.5$ eV) and is consistent with the fact that the adsorbed alkali-metal atom is not fully ionized.

When an alkali-metal atom is brought into the vicinity of a metal surface, the ns and np levels shift (see above) and broaden into resonances. The ns resonance is located mainly above the Fermi energy but also has a tail extending below this energy. Theoretical first-principles calculations have shown that the ns resonance at low alkali-metal coverage is centered ~ 2 eV above E_F and has a full width at half maximum (FWHM) $\Gamma_s\sim 1$–2 eV.[8] Hence the filling of the ns resonance (accounting for both spin directions) is typically ~ 0.2 electron as compared with one electron in the gas phase. We note here that a partial filling of the ns resonance, even at very low alkali-metal coverage, is in accordance with the metastable helium deexcitation data of Woratschek *et al.*[6]

As the alkali-metal coverage increases, the dipole moments associated with the partly ionized alkali-metal atoms and their images will give rise to an electric potential at the surface which shifts the ns and np levels towards larger binding energies. This will increase the occupation of the ns resonance and hence decrease the dipole moment associated with an alkali-metal atom. The alkali-metal-induced electric field at the surface also has a second effect: due to the nonzero static polarizability associated with virtual electronic transitions from the filled part of the ns resonance to the empty np resonance, dipole moments will be induced in the alkali-metal atoms which have opposite direction to that caused by the $ns\rightarrow$metal charge transfer. Both of these effects must be accounted for when describing the coverage-dependent work function. Note, however, that at low alkali-metal coverage, owing to the small occupation of the ns resonance, the contribution to the polarizability from virtual $ns\rightarrow np$ transitions will be much smaller than for gas phase alkali-metal atoms (see below).

The processes described above are contained in the following model Hamiltonian:[7]

$$H_0=\varepsilon_s\hat{n}_s+\varepsilon_p\hat{n}_p+\sum_k\varepsilon_k\hat{n}_k+\sum_k(V_{sk}c_s^\dagger c_k+\text{H.c.})+\sum_k(V_{pk}c_p^\dagger c_k+\text{H.c.})-\hat{\mu}\cdot E_0\ . \quad (1)$$

Here, we consider one single adsorbed alkali-metal atom which interacts with the other adsorbed alkali-metal atoms only via the local electric field E_0 to be specified later. The energy levels ε_s and ε_p are "renormalized" due to, e.g., image effects and we have neglected the Coulomb repulsion energy U associated with having two electrons (spin up and spin down) in the s level (it has been argued by Muscat and Newns[7] that the *effective* U for adsorbed alkali-metal atoms is negligibly small). The energy levels of the metal are denoted by ε_k, and V_{sk} and V_{pk} denote the hybridization interaction between the $|ns\rangle$ and $|np_z\rangle$ orbitals and the metal orbitals $|k\rangle$. Finally, the dipole moment operator $\hat{\mu}$ is given by

$$\hat{\mu}=ed(0.5-\hat{n}_s-\hat{n}_p)+e\lambda(c_s^\dagger c_p+c_p^\dagger c_s)\ . \quad (2)$$

We have assumed spin degeneracy. For later use, we note that if a time-dependent external electric field $E(t)$ exists at the surface, we must add the term $-\hat{\mu}\cdot E(t)$ to (1) [throughout this paper we will assume that the time dependence of any external field $E(t)\sim\exp(-i\omega t)$ is so slow that the metal electrons can screen it out almost perfectly inside the metal, i.e., we assume that $\omega\ll\omega_p$, where ω_p is the bulk plasma frequency].

III. WORK FUNCTION

The work-function change $\Delta\phi$ induced by adsorption of alkali-metal atoms on a surface is given by

$$\Delta\phi=4\pi nep\ , \quad (3)$$

where n is the number of adsorbed alkali-metal atoms per unit area. The dipole moments of all the adsorbed alkali-metal atoms are assumed identical, which is the case only if they form an ordered lattice structure. At low alkali-metal coverage and at high enough temperature, where the thermal motion can overcome the strong repulsive interaction between the alkali-metal atoms, this

is no longer the case (we will discuss temperature effects in Sec. VI). We can write

$$p = \langle \psi | \hat{\mu} | \psi \rangle$$

where $|\psi\rangle$ is the ground state of the adsorbate system. Since the Hamiltonian (1) is an effective one-particle Hamiltonian, it can easily be diagonalized, and p and $\Delta\phi$ can consequently be calculated exactly within this model.[7] Here we prefer to present an approximate solution which is strictly valid only at low adsorbate coverage, but which is easier to interpret physically.

We assume that the np resonance remains unoccupied upon adsorption. The dipole moment p then has only two contributions:

$$p = p_s + \alpha_{sp}(0) E_0 \ , \tag{4}$$

where p_s is the contribution from the alkali-metal→metal charge transfer, i.e.,

$$p_s = ed(1 - 2\langle \hat{n}_s \rangle) \ , \tag{5}$$

and where $\alpha_{sp}(0)$ is the static polarizability associated with virtual electronic transitions from the filled part of the ns resonance to the np resonance. E_0 is the electric field at the adsorbate under study from the dipoles associated with all the other adsorbed alkali-metal atoms, i.e.,

$$E_0 \approx - \sum_{i \neq 0} \frac{2p}{|\mathbf{x}_i|^3} = -Up \ , \tag{6}$$

where $U \approx 18 n^{3/2}$ and where the factor of 2 accounts for the image dipoles. If $\rho_s(\varepsilon)$ denotes the density of states projected on the ns resonance, then

$$\langle n_s \rangle = \int_{-\infty}^{\varepsilon_F} d\varepsilon \, \rho_s(\varepsilon) \ . \tag{7}$$

Note that

$$\int_{-\infty}^{\infty} d\varepsilon \, \rho_s(\varepsilon) = 1 \ .$$

The polarizability α_{sp} is calculated in Sec. IV where it is found

$$\alpha_{sp}(\omega) = 2(e\lambda)^2 \int_{-\infty}^{\varepsilon_F} d\varepsilon \int_{-\infty}^{\infty} d\varepsilon' \rho_s(\varepsilon) \rho_p(\varepsilon') \left[\frac{1}{\varepsilon' - \varepsilon - \omega - i0} - \frac{1}{\varepsilon - \varepsilon' - \omega - i0} \right] , \tag{8}$$

and the static polarizability $\alpha_{sp}(0)$ is obtained by setting $\omega = 0$ in (8).

In all of the numerical results presented in this paper, we have assumed that $\rho_s(\varepsilon)$ and $\rho_p(\varepsilon)$ are Lorentzians, i.e.,

$$\rho_s(\varepsilon) = \frac{1}{\pi} \frac{\Gamma_s/2}{(\varepsilon - \varepsilon_s - edE_0)^2 + (\Gamma_s/2)^2} \tag{9}$$

and

$$\rho_p(\varepsilon) = \frac{1}{\pi} \frac{\Gamma_p/2}{(\varepsilon - \varepsilon_p - edE_0)^2 + (\Gamma_p/2)^2} \ . \tag{10}$$

Furthermore, we assume that λ and the separation $\varepsilon_s - \varepsilon_p$ between the ns and np levels are the same as in the gas phase. The free parameters in the theory are therefore d, $\varepsilon_s - \varepsilon_F$, and Γ_s and Γ_p (most results presented below are rather insensitive to the width Γ_p of the np resonance). These parameters have been chosen to give the best possible fit to the known coverage-dependent work function for K on Cu(100).[9]

Substituting (5)–(10) into (4) gives an implicit expression for p as a function of coverage n, which can be solved for $p(n)$ by iteration. The circles in Fig. 1 show the variation in the work function ϕ with the coverage n for K on Cu(100) (Ref. 9) at $T = 120$ K. The K-monolayer coverage is at $n \approx 0.057$ Å^{-2}. The solid line has been calculated using the theory described above with $d = 1.9$ Å, $\varepsilon_s - \varepsilon_F = 2.4$ eV, and $\Gamma_s = \Gamma_p = 1$ eV (and from gas phase data, $\lambda = 1.41$ Å and $\varepsilon_p - \varepsilon_s = 1.6$ eV). The dashed line is obtained with the same parameters as above except that we have put $\lambda = 0$ so that no screening associated with $s \rightarrow p$ transitions can occur. As expected, the dipole moment p now becomes larger.

The parameter values used above are quite reasonable. For example, the value of d is very similar to what one would obtain using the Lang-Kohn reference plane for the image potential[10] and the width $\Gamma = 1$ eV is in accordance with the calculations by Muscat and Batra.[11]

To illustrate the physics involved in more detail, let us consider the coverage dependence of $\varepsilon_s - edE_0 - \varepsilon_F \equiv \tilde{\varepsilon}_s - \varepsilon_F$, $\alpha_{sp}(0)$, and the filling $\langle n_s \rangle$ of the ns resonance.

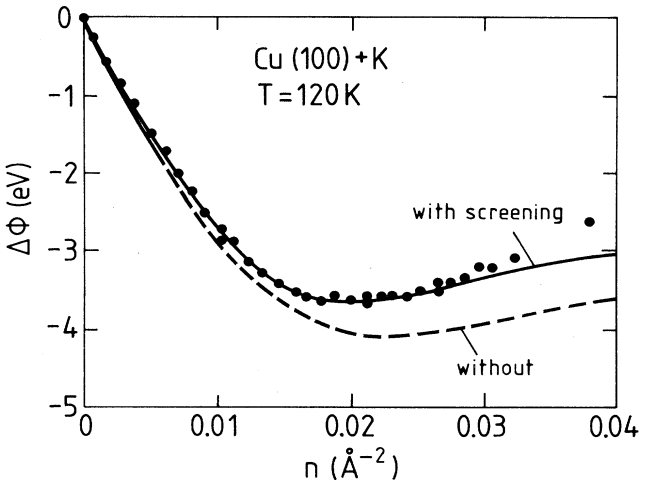

FIG. 1. The work-function change $\Delta\phi$ as a function of coverage n for K on Cu(100). The circles are experimental data from Dubois *et al.* (Ref. 9). The two curves are theoretical results calculated with and without the screening caused by virtual $s \rightarrow p$ transitions. The model parameters are $d = 1.9$ Å, $\varepsilon_s - \varepsilon_F = 2.4$ eV, $\Gamma_p = \Gamma_s = 1$ eV and from gas phase K, $\varepsilon_p - \varepsilon_s = 1.6$ eV, and $\lambda = 1.41$ Å (with $s \rightarrow p$ screening) and $\lambda = 0$ (without $s \rightarrow p$ screening).

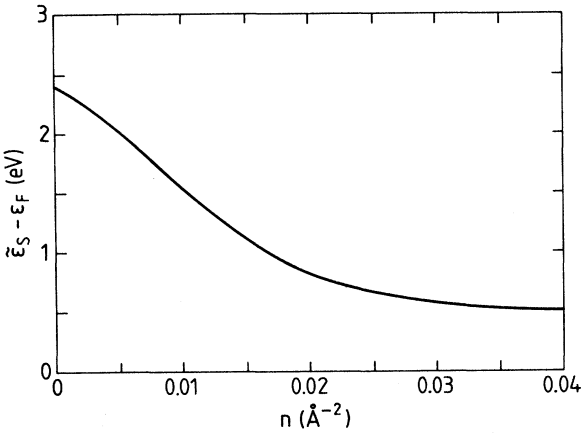

FIG. 2. The separation $\tilde{\varepsilon}_s - \varepsilon_F$ between the center of the s resonance and the Fermi energy (note: $\tilde{\varepsilon}_s = \varepsilon_s - edE_0$) as a function of the coverage n of K adatoms. The same model parameters as in Fig. 1 (with screening).

Figures 2 and 3 show the coverage dependence of $\tilde{\varepsilon}_s - \varepsilon_F$ and $2\langle n_s \rangle$, respectively. As expected, these quantities change monotonically with increasing coverage. The dashed line in Fig. 3 shows the variation of $2\langle n_s \rangle$ in a second calculation where we have set $\lambda = 0$ *and* readjusted the other parameter values ($d = 2.2$ Å, $\Gamma_s = 1.5$ eV, and $\varepsilon_s - \varepsilon_F = 2.4$ eV) so that the experimental work-function data in Fig. 1 are still well reproduced. We note that the filling of the s resonance in this latter case is larger, i.e., the net dipole moment caused by charge transfer is smaller than before. The reason for this is obvious—in order to have the same total dipole moment p [Eq. (4)] in the absence of screening by $s \rightarrow p$ transitions, it is necessary to reduce the charge transfer from the alkali-metal *ns* level to the metal.

Let us now consider Fig. 4, which shows the variation of the static $s \rightarrow p$ polarizability, $\alpha_{sp}(0)$, with the position

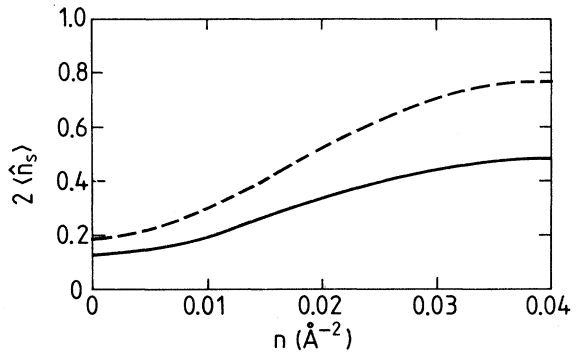

FIG. 3. The occupation of the s resonance (including both spin directions) as a function of the alkali-metal coverage n. The solid curve has been calculated using the same parameters as in Fig. 1 while the dashed curve is obtained with $\lambda = 0$, i.e., without screening from virtual $s \rightarrow p$ transitions. The other model parameters are readjusted so that the coverage-dependent work-function data in Fig. 1 can be well fitted ($d = 2.2$ Å, $\Gamma_s = 1.5$ eV, and $\varepsilon_s - \varepsilon_F = 2.4$ eV).

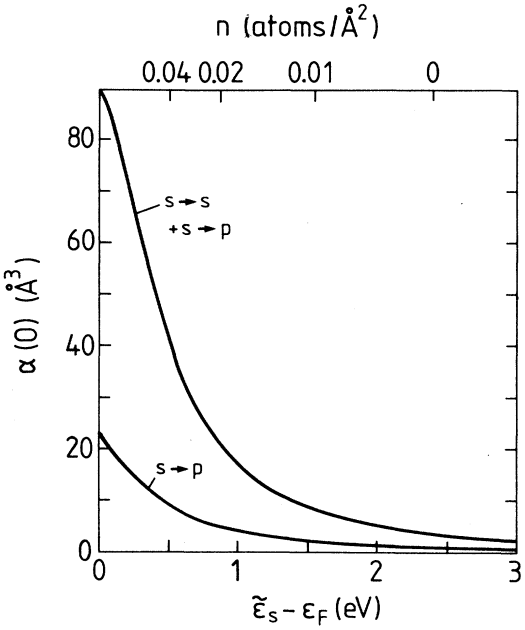

FIG. 4. The total static electronic polarizability (curve denoted by $s \rightarrow s + s \rightarrow p$) and the contribution from $s \rightarrow p$ transitions alone, as a function of the alkali-metal coverage. The same model parameters as in Fig. 1.

of the *ns* resonance relative to the Fermi energy (lower scale) and as a function of K coverage (upper scale). The separation between the s and p resonances is kept constant at 1.4 eV. As $\tilde{\varepsilon}_s - \varepsilon_F$ decreases, the polarizability $\alpha_{sp}(0)$ increases. This is partly a result of the increasing occupation of the *ns* resonance and partly because the separation between the Fermi energy and the center of the *np* resonance decreases leading to smaller virtual excitation energies [see (8)]. Note also that the static polarizability $\alpha_{sp}(0)$ in the case of a half-filled *ns* resonance (i.e., $\tilde{\varepsilon}_a - \varepsilon_F = 0$) is smaller than that of a gas phase K atom (23 versus 36 Å^3). This is a result of the nonzero width of the *ns* and *np* resonances which increases the average virtual $s \rightarrow p$ excitation energies involved in the polarizability (8) [when Γ_s and $\Gamma_p \rightarrow 0$, (8) reproduces the gas phase polarizability].

It is interesting to note that the main part of the static polarizability of an adsorbed alkali-metal atom comes not from the $s \rightarrow p$ transitions but rather from virtual transitions from the filled part of the s resonance to the empty part of the same resonance. Indeed, the *total* static polarizability is much larger (90 Å^3, see Fig. 4) than the gas phase polarizability (36 Å^3). Note also that at small alkali-metal coverage, where the filling of the *ns* resonance is small, the polarizabilities derived from the $s \rightarrow p$ transitions are very small (e.g., $\alpha_{sp} \approx 1$ Å^3 as $n \rightarrow 0$).

IV. POLARIZABILITY

The frequency-dependent polarizability of adsorbates can be studied using electron-energy-loss spectroscopy. Hence we will first review some of the basic equations which relate to EELS.[12]

Let us first define the surface response function $g(\mathbf{q}_\parallel,\omega)$ which plays an important role in EELS. Consider a semi-infinite medium occupying the half-space $z>0$. Let

$$\phi_{\rm ext}(\mathbf{x},t)=e^{i\mathbf{q}_\parallel\cdot\mathbf{x}_\parallel-q_\parallel z-i\omega t} \tag{11}$$

be an external potential which polarizes the medium. The induced polarization changes will give rise to an induced potential which for $z<0$ (i.e., outside the medium) can be written as

$$\phi_{\rm ind}(\mathbf{x},t)=-g(\mathbf{q}_\parallel,\omega)e^{i\mathbf{q}_\parallel\cdot\mathbf{x}_\parallel+q_\parallel z-i\omega t} . \tag{12}$$

This equation defines $g(\mathbf{q}_\parallel,\omega)$.

Now consider an electron incident upon the surface. The electric field from the electron penetrates into the medium where it can excite, e.g., electron-hole pairs, plasmons, or phonons. Let $\mathbf{k}$ and $\mathbf{k}'$ denote the wave vectors of an incident and an inelastically scattered electron, respectively. Thus $\hbar\mathbf{q}_\parallel=\hbar(\mathbf{k}_\parallel-\mathbf{k}'_\parallel)$ is the momentum transfer (parallel to the surface) to the excitation in the medium and $\hbar\omega=\hbar^2(k^2-k'^2)/2m$ is the energy transfer. Let $P(\mathbf{k},\mathbf{k}')d\Omega_{k'}d(\hbar\omega)$ be the probability that an incident electron is scattered inelastically into the range of energy losses between $\hbar\omega$ and $\hbar(\omega+d\omega)$, and into the solid angle $d\Omega_{k'}$ around the direction of $\mathbf{k}'$. For small momentum transfer, $q_\parallel\ll k$, and for "weak" scattering one has, from standard dipole scattering theory,

$$P(\mathbf{k},\mathbf{k}')=\frac{2}{(ea_0\pi)}\frac{1}{\cos\alpha}\frac{k}{k'}\frac{q_\parallel}{|q_\parallel^2+q_\perp^2|^2}\,\mathrm{Img}(\mathbf{q}_\parallel,\omega) ,$$

$$\equiv A(\mathbf{k},\mathbf{k}')\,\mathrm{Img}(\mathbf{q}_\parallel,\omega) , \tag{13}$$

where $q_\perp=k_z-k'_z$, and α is the angle of incidence. Thus the inelastic scattering probability is a product of two factors—a kinematic factor $A(\mathbf{k},\mathbf{k}')$ which is independent of the properties of the medium, and the loss function $\mathrm{Img}(\mathbf{q}_\parallel,\omega)$ which is proportional to the power absorption in the medium due to an external potential of the form (11). $g(\mathbf{q}_\parallel,\omega)$ enters the inelastic scattering probability (13) because it determines the induced electric field outside the substrate [via (12)] and it is this time-varying field that can scatter the incident electron inelastically.

For a regular lattice of atoms, treated as point particles with the polarizability $\alpha(\omega)$, adsorbed on a substrate described by a local dielectric function $\epsilon(\omega)$, one can show that (see Appendix A)

$$g=\frac{\epsilon(\omega)-1}{\epsilon(\omega)+1}+8\pi nq_\parallel\alpha_0(\mathbf{q}_\parallel,\omega) . \tag{14}$$

The total polarizability $\alpha_0(\mathbf{q}_\parallel,\omega)$ is given by

$$\alpha_0(\mathbf{q}_\parallel,\omega)=\frac{\alpha(\omega)}{1+\alpha(\omega)U(\mathbf{q}_\parallel)} , \tag{15}$$

where

$$U(\mathbf{q}_\parallel)=\sum_i{}'\frac{2}{|\mathbf{x}_i|^3}e^{i\mathbf{q}_\parallel\cdot\mathbf{x}_i} \tag{16}$$

and the factor of 2 accounts for image dipoles. Equation (14) assumes that $|\epsilon(\omega)|\gg1$ (which for a free-electron metal requires $\omega\ll\omega_p$, where ω_p is the plasma frequency). This approximation is satisfied in the applications presented below.

Let us now calculate the polarizability of an adsorbed alkali-metal atom within the model described in Sec. II. Let $E(t)$ be an external time-varying electric field. The Hamiltonian for the adsorbate system is given by

$$H=H_0-\hat{\mu}\cdot E(t) , \tag{17}$$

where H_0 and $\hat{\mu}$ are given by (1) and (2). Since H_0 is quadratic in creation and annihilation operators, it can be diagonalized

$$H_0=\sum_\alpha\varepsilon_\alpha c_\alpha^\dagger c_\alpha . \tag{18}$$

In the new basis

$$\hat{\mu}=\sum_{\alpha\beta}\mu_{\alpha\beta}c_\alpha^\dagger c_\beta , \tag{19}$$

where $\mu_{\alpha\beta}=\langle\alpha|\hat{\mu}|\beta\rangle$. Accounting for both spin directions, the polarizability $\alpha(\omega)$ is given by the standard formula

$$\alpha(\omega)=2\sum_{\alpha\beta}f(\varepsilon_\alpha)\mu_{\alpha\beta}\mu_{\beta\alpha}\times\left[\frac{1}{\varepsilon_\beta-\varepsilon_\alpha-\omega-i0}-\frac{1}{\varepsilon_\alpha-\varepsilon_\beta-\omega-i0}\right] , \tag{20}$$

where $f(\varepsilon_\alpha)=1$ if $\varepsilon_\alpha<\varepsilon_F$ and zero otherwise. Using (2), we can write ($\alpha\neq\beta$)

$$\mu_{\alpha\beta}=-ed\langle\alpha|s\rangle\langle s|\beta\rangle+\lambda e(\langle\alpha|s\rangle\langle p|\beta\rangle+\langle\alpha|p\rangle\langle s|\beta\rangle) . \tag{21}$$

Substituting (21) into (20) gives

$$\alpha(\omega)=2\int d\varepsilon\,d\varepsilon' f(\varepsilon)\rho_s(\varepsilon)[(ed)^2\rho_s(\varepsilon')+(e\lambda)^2\rho_p(\varepsilon')]\times\left[\frac{1}{\varepsilon'-\varepsilon-\omega-i0}-\frac{1}{\varepsilon-\varepsilon'-\omega-i0}\right] , \tag{22}$$

where

$$\rho_s(\varepsilon)=\sum_\alpha|\langle\alpha|s\rangle|^2\delta(\varepsilon-\varepsilon_\alpha)$$

and

$$\rho_p(\varepsilon)=\sum_\alpha|\langle\alpha|p\rangle|^2\delta(\varepsilon-\varepsilon_\alpha) .$$

In deriving (22) we have made two assumptions.

(a) The occupation of the *np* resonance can be neglected.

(b) Terms involving

$$\rho_{sp}(\varepsilon)=\sum_\alpha\langle s|\alpha\rangle\langle\alpha|p\rangle\delta(\varepsilon-\varepsilon_\alpha)$$

can be neglected compared with terms involving $\rho_s(\varepsilon)$ or $\rho_p(\varepsilon)$. This assumption is a good approximation if, e.g., the overlap between ρ_s and ρ_p is small (see Appendix B).

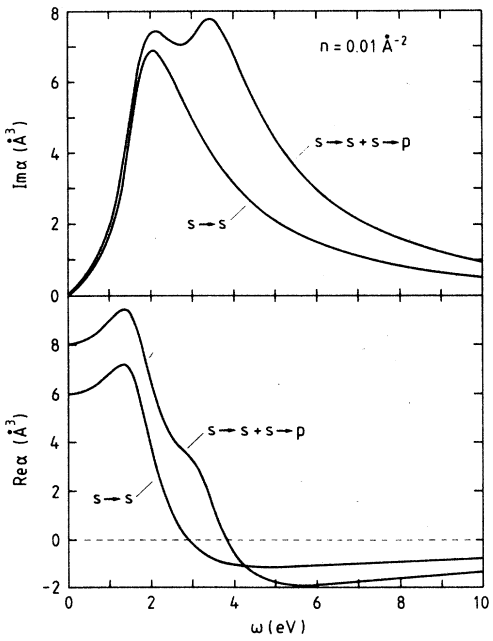

FIG. 5. The real and imaginary part of the single-particle polarizability $\alpha(\omega)$ as a function of the frequency ω of the external driving field. The calculation is for the alkali-metal coverage $n=0.01$ Å^{-2} using the same model parameters as in Fig. 1. The curve denoted by $s\rightarrow s+s\rightarrow p$ is the total polarizability while the other curve shows the contribution from $s\rightarrow s$ transitions alone.

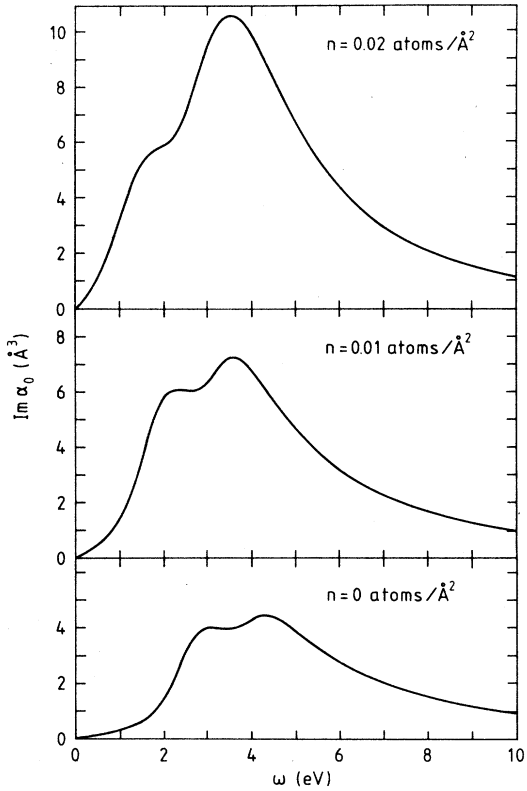

FIG. 6. The total polarizability $\alpha_0(\mathbf{q}_\parallel,\omega)$ for $q_\parallel=0$ as a function of frequency ω and for several alkali-metal coverages.

Let us now present some numerical results. We assume that ρ_s and ρ_p are Lorentzians [see (9) and (10)] and that all the parameters ε_s, ε_p, Γ_s, Γ_p, λ, and d take the same values as before. Figure 5 shows the real and imaginary parts of the polarizability $\alpha(\omega)$ of a single particle at the coverage $n=0.01$ Å^{-2}. At small frequencies, the contribution from $s\rightarrow s$ transitions dominates, particularly for Imα. Figure 6 shows the imaginary part of the total polarizability [as given by (15)] with $q_\parallel=0$ and for three different coverages, $n=0$, 0.01, and 0.02 Å^{-2}. For later use, we present both the magnitude and the phase of the screening factor $(1+\alpha U)^{-1}$ in Fig. 7.

Let us now compare theory with experiment. Many EELS experiments have been performed on alkali-metal atoms adsorbed on transition metals, noble metals, and on aluminum. Here, we will only focus on the low alkali-metal-coverage regime. All of the experimental data exhibit a peak at ~ 3 eV loss energy with a full width at half maximum of a few eV. Since the adsorbate-induced EELS signal is proportional to Imα_0 (we assume that dipole coupling dominates the inelastic scattering cross section), one expects theoretically and finds experimentally, spectra in rough agreement with the results given in Fig. 6. A crucial test of the theory is whether the theoretically predicted intensity of the loss peak is in accordance with the experimental data. To test this we consider the experimental results of Andersson and Jostell[2] for K on Ni(100). At a K coverage of about

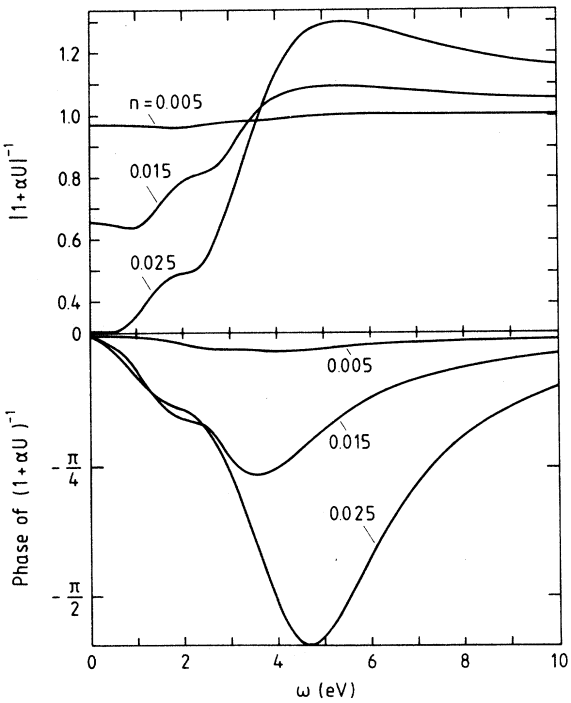

FIG. 7. The absolute magnitude and the phase of the screening factor $(1+\alpha U)^{-1}$ as a function of frequency ω and for several alkali-metal coverages.

0.016 Å^{-2} the *increase* in the EELS signal at the maximum of the loss peak is roughly a factor of 2 larger than that of the clean surface at the same loss energy (see Fig. 8), i.e., using (14)

$$\frac{8\pi n q_{\parallel}\,\mathrm{Im}\alpha_0(q_{\parallel},\omega)}{\mathrm{Im}[\epsilon(\omega)-1]/[\epsilon(\omega)+1]}\approx 2\ . \tag{23}$$

In dipole scattering, $q_{\parallel}\approx(\hbar\omega/2E_0)k_0$ and using the tabulated dielectric function $\epsilon(\omega)$ for Ni at $\hbar\omega=2.3$ eV, we get $\mathrm{Im}(\varepsilon-1)/(\varepsilon+1)\approx 0.14$ eV and (23) gives

$$\mathrm{Im}\alpha_0\approx\frac{\mathrm{Im}(\varepsilon-1)/(\varepsilon+1)}{4\pi n\hbar\omega k_0/2E_0}\approx 6\ \text{Å}^3\ ,$$

where we have used $E_0=18$ eV. This is in rough agreement with $\mathrm{Im}\alpha_0\approx 10\ \text{Å}^3$ at the peak maximum in Fig. 6. Hence we conclude that it is very likely that the loss peaks observed in EELS from adsorbed alkali-metal atoms in the low coverage regime are due to electronic transitions from the occupied part of the *ns* resonance to the unoccupied part of the same resonance and to the *np* resonance.

Finally, let us present another test of the theory. Inelastic scattering of slow electrons from metal surfaces is an ideal tool for the study of the low-energy surface excitations. Recently, this technique has been used to study the electron-hole pair response of a Cu(100) surface.[13] There are several contributions to the loss function $\mathrm{Im}g(\mathbf{q}_{\parallel},\omega)$ which can be classified according to the source of the momentum needed for the excitations. Here, we will focus only on the surface contribution where the momentum needed for the excitation comes from the surface potential. It has been shown that within the semi-infinite jellium model

$$\mathrm{Im}g|_{\mathrm{surf}}=2\xi\frac{q_{\parallel}}{k_F}\frac{\omega}{\omega_p}\ , \tag{24}$$

where, for Cu($r_s=2.67$), $2\xi\approx 1$. Now, when a low coverage of alkali-metal atoms is adsorbed on the surface, there will be another contribution to Img which is given by the second term in (14)

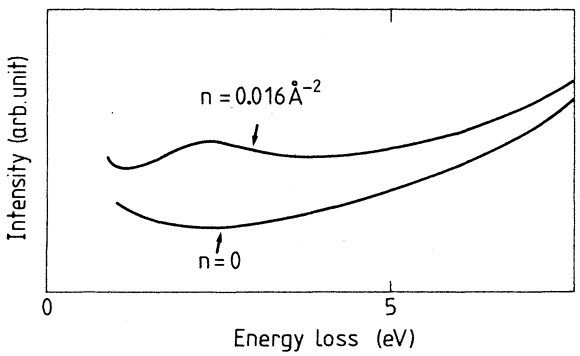

FIG. 8. Experimental electron-energy-loss spectra from K on Ni(100) for two alkali-metal coverages, $n=0$ and 0.016 atoms Å^{-2}. From Andersson and Jostell, Ref. 2.

$$\mathrm{Im}g|_{\mathrm{alkali}}=8\pi n q_{\parallel}\,\mathrm{Im}\alpha_0\ . \tag{25}$$

Hence

$$\frac{\mathrm{Im}g|_{\mathrm{alkali}}}{\mathrm{Im}g|_{\mathrm{surf}}}=nk_F\omega_p\frac{4\pi}{\xi}\frac{\mathrm{Im}\alpha_0}{\omega}\ . \tag{26}$$

For small ω, $\mathrm{Im}\alpha_0\sim\omega$ so that (26) is ω independent. For, e.g., $n=0.02\ \text{Å}^{-2}$ we have from Fig. 6 $\mathrm{Im}\alpha_0\approx 2\omega$ where ω is measured in eV and α_0 is in Å^3. Hence (26) gives (for a Cu substrate)

$$\frac{\mathrm{Im}g|_{\mathrm{alkali}}}{\mathrm{Im}g|_{\mathrm{surf}}}\approx 15\ .$$

We conclude that a metal surface with a low concentration of alkali-metal atoms is much more "lossy" at low frequencies than the clean surface. (Note, however, that care must be taken to minimize the contribution from the bulk and interference processes, as discussed in Ref. 13.) To test this theoretical prediction we have performed inelastic scattering of slow electrons from the K/Cu(100) system.

The thin lines in Figs. 9(a), 9(b), and 9(c) show the inelastic electron-hole pair background for a clean surface and for two K-covered surfaces, $n=0.0077$ and 0.017 Å^{-2}. The solid line in 9(a) (clean surface) is the theoretically predicted loss background for Cu where we have included the surface, bulk, and interference contribution to Img [see Ref. 13(b) for details]. This first-principles calculation, which contains no adjustable parameters, agrees very well with the experimental data for loss energies above ≈ 0.1 eV. The deviation between theory and experiment for small loss energies is attributed to trace amounts of C and O impurities. The experiment has been performed under such conditions that the bulk and interference contribution to Img cancel almost exactly [see Fig. 6 in Ref. 13(b)]; hence the solid line in Fig. 9(a) directly represents the surface contribution to the inelastic loss background. The solid curves in 9(b) and 9(c) give the expected loss background under the assumption that $\mathrm{Im}\alpha_0\sim\omega$. We have scaled these curves so that they agree with the experimental data at small loss energies. For case (b) of Ref. 9 relatively good agreement between theory and experiment is obtained although the experimental data tend to decay somewhat slower with increasing loss energy than the theoretical result. For case (c) of Fig. 9 the discrepancy between theory and experiment is much larger, the experimental data now lying well above the theoretical result for large loss energies. We attribute this deviation between theory and experiment to nonlinear contributions to $\mathrm{Im}\alpha_0(\omega)$. Indeed from Fig. 6 it is obvious that for "large" ω, $\mathrm{Im}\alpha_0$ increases faster than indicated by the initial linear slope. The "onset" of this rapid increase in $\mathrm{Im}\alpha_0(\omega)$ occurs at smaller loss energies ω as the potassium coverage increases, in qualitative agreement with the experimental data in Fig. 9. The magnitude of the loss background at small loss energies is also in good agreement with theory. The solid lines in 9(b) and 9(c) are obtained by scaling the solid line in 9(a) with the factors 3.5 and 14, respectively. Subtracting away the contribution from the clean surface (we assume

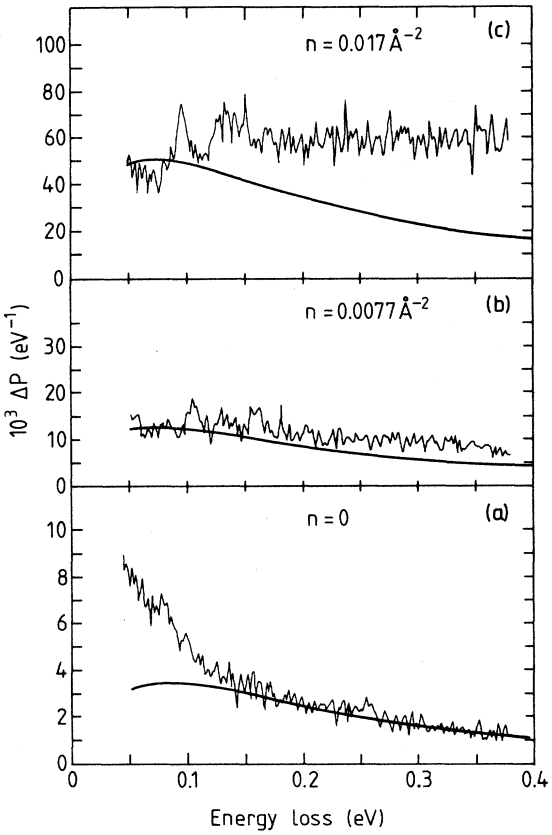

FIG. 9. The electron-hole pair signal ΔP as a function of the loss energy and for three different coverages n of K on Cu(100). The solid line for the clean surface ($n=0$) is the theoretical result obtained using an incident electron energy $E_0=1.7$ eV, an angle of incidence $\alpha=60°$, and a collection angle for the analyzer (half-width at half maximum) 2°. The thick solid lines for the alkali-metal-covered surfaces have been obtained by scaling that of the clean surface with factors 3.5 and 14. Experimental details are discussed in Ref. 9.

additivity) this gives enhancement factors of 2.5 and 13. By interpolation from Fig. 6 we obtain $\mathrm{Im}\alpha_0 \approx 0.8\omega$ and $\mathrm{Im}\alpha_0 \approx 1.6\omega$ for the potassium coverages $n=0.0077$ and 0.017 Å^{-2}, respectively, where ω is measured in eV and α_0 in Å^3. Substituting these results in (26) gives the enhancement factors 2.3 and 10.2, respectively, which is in remarkably good agreement with those deduced from the experimental data.

Finally let us point out that Eguiluz and Campbell have performed a very nice and detailed study of the dynamical response of thin jellium slabs on a jellium substrate.[14] However, these calculations are of no relevance for the present work which is concerned with low alkali-metal coverages which cannot be described by a uniform jellium slab.

V. SECOND-HARMONIC GENERATION

Second-harmonic generation has found increasing application in surface science because of its surface sensitivity.[15] SHG vanishes in systems with inversion symmetry, e.g., in the bulk of simple metals, but not at the crystal surface where the inversion symmetry is broken.

SHG has been used to study clean metal and semiconductor surfaces,[16] as well as adsorption of gases on metal surfaces.[17] It can often be used under conditions where many standard surface-science techniques cannot be applied, e.g., to study surfaces in liquids or interfaces between solids. In addition, the method has inherently high time resolution limited only by the pulse duration of the laser employed (which currently can be shorter than 10^{-13} s).

Recently, tremendously enhanced SHG signals have been observed for thin layers of alkali metals adsorbed on noble- and transition-metal surfaces.[4,5] In particular, Song *et al.* find that less than one monolayer of Rb on Ag(110) enhances the SHG signal by a factor ~ 1000 at the incident photon energy $\hbar\omega=1.16$ eV. Here, we show that the simple model described in Sec. II gives a strong enhancement at low alkali-metal coverage.

Let $E(t)$ be an "external" time-varying electric field. The Hamiltonian for the adsorbate system is written as before

$$H=H_0-\hat{\mu}\cdot E(t)\ , \tag{27}$$

where H_0 and $\hat{\mu}$ are given by (1) and (2). As before, we introduce a new basis in which the one-particle operator H_0 is diagonal:

$$H_0=\sum_\alpha \varepsilon_\alpha c_\alpha^\dagger c_\alpha\ . \tag{28}$$

In this basis

$$\hat{\mu}=\sum_{\alpha\beta}\mu_{\alpha\beta}c_\alpha^\dagger c_\beta\ , \tag{29}$$

$$\mu_{\alpha\beta}=-ed\langle\alpha|s\rangle\langle s|\beta\rangle + \lambda e(\langle\alpha|s\rangle\langle p|\beta\rangle+\langle\alpha|p\rangle\langle s|\beta\rangle)\ . \tag{30}$$

Second-order response theory gives the second-order induced dipole moment as (at zero temperature)

$$P_2(t)=\int dt\,dt'\chi(t,t',t'')E(t')E(t'')\ , \tag{31}$$

where

$$\chi=-\Theta(t-t')\Theta(t'-t'')\langle 0|[[\hat{\mu}(t),\hat{\mu}(t')],\hat{\mu}(t'')]|0\rangle\ , \tag{32}$$

where $|0\rangle$ is the ground state of the system in the absence of the "external" field $E(t)$. Substituting (29) into (32) gives

$$\chi(t,t',t'')=-\Theta(t-t')\Theta(t'-t'')\times\sum_\alpha n_\alpha[[\mu(t),\mu(t')],\mu(t'')]_{\alpha\alpha}\ , \tag{33}$$

where the matrix $\mu(t)$ has the components

$$\mu_{\alpha\beta}(t)=\mu_{\alpha\beta}e^{i(\varepsilon_\alpha-\varepsilon_\beta)t}\ . \tag{34}$$

It is convenient to Fourier transform the time dependence

$$E(t)=\int d\omega\, E(\omega)e^{-i\omega t}\ , \tag{35}$$

$$E(\omega)=\frac{1}{2\pi}\int dt\, E(t)e^{i\omega t}\ , \tag{36}$$

and similarly for $p(t)$. Substituting this into (31) gives

$$P_2(\omega)=\int d\omega' d\omega''\chi(\omega,\omega',\omega'')E(\omega')E(\omega'')\ , \tag{37}$$

where

$$\chi(\omega,\omega',\omega'')=\frac{1}{2\pi}\int dt\, dt' dt'' e^{i(\omega t-\omega' t'-\omega'' t'')}\chi(t,t',t'')\ . \tag{38}$$

Substituting (33) and (34) into (38) gives

$$\chi(\omega,\omega',\omega'')=\delta(\omega-\omega'-\omega'')A(\omega,\omega'')\ , \tag{39}$$

where

$$A(\omega,\omega'')=\int d\varepsilon\, d\varepsilon' d\varepsilon'' f(\varepsilon)F(\varepsilon,\varepsilon',\varepsilon'')\left[\frac{1}{\omega+\varepsilon-\varepsilon'+i0}\frac{1}{\omega''+\varepsilon-\varepsilon''+i0}+\frac{1}{\omega+\varepsilon''-\varepsilon+i0}\frac{1}{\omega''+\varepsilon'-\varepsilon+i0}\right.$$
$$\left.-\frac{1}{\omega+\varepsilon'-\varepsilon''+i0}\frac{1}{\omega''+\varepsilon-\varepsilon''+i0}-\frac{1}{\omega+\varepsilon'-\varepsilon''+i0}\frac{1}{\omega''+\varepsilon'-\varepsilon+i0}\right]\ , \tag{40}$$

where

$$F=2\sum_{\alpha\beta\gamma}\mu_{\alpha\beta}\mu_{\beta\gamma}\mu_{\gamma\alpha}\delta(\varepsilon-\varepsilon_\alpha)\delta(\varepsilon'-\varepsilon_\beta)\delta(\varepsilon''-\varepsilon_\gamma)\ , \tag{41}$$

where the factor of 2 accounts for the electron spin.

Substituting (30) into (41) gives

$$F=2(-ed)^3\rho_s(\varepsilon)\rho_s(\varepsilon')\rho_s(\varepsilon'')+2(e\lambda)^2(-ed)\rho_s(\varepsilon)[\rho_s(\varepsilon')\rho_p(\varepsilon'')+\rho_p(\varepsilon')\rho_s(\varepsilon'')]\ . \tag{42}$$

In deriving this formula, we have made the same two approximations as in Sec. III, namely, (a) we have assumed that the occupation of the p resonance is negligible; (b) we have neglected terms involving $\rho_{sp}(\varepsilon)$ which is a good approximation if the overlap between $\rho_s(\varepsilon)$ and $\rho_p(\varepsilon)$ is small (see Appendix B).

If ρ_s and ρ_p are well approximated by Lorentzians [see (9) and (10)], then the ε' and ε'' integrals can be performed analytically. The remaining integral over ε is conveniently performed by numerical integration.

Let us now assume that the "external" electric field has the form

$$E(t)=E_0e^{-i\omega_0 t}+E_0^*e^{i\omega_0 t}$$

so that

$$E(\omega)=E_0\delta(\omega-\omega_0)+E_0^*\delta(\omega+\omega_0)\ .$$

Substituting this into (36) gives an integrand proportional to

$$\delta(\omega-\omega'-\omega'')[E_0\delta(\omega'-\omega_0)+E_0^*\delta(\omega'+\omega_0)][E_0\delta(\omega''-\omega_0)+E_0^*\delta(\omega''+\omega_0)]$$
$$=\delta(\omega-2\omega_0)E_0^2\delta(\omega'-\omega_0)\delta(\omega''-\omega_0)+\delta(\omega+2\omega_0)(E_0^*)^2\delta(\omega'+\omega_0)\delta(\omega''+\omega_0)$$
$$+\delta(\omega)E_0E_0^*[\delta(\omega'-\omega_0)\delta(\omega''+\omega_0)+\delta(\omega'+\omega_0)\delta(\omega''-\omega_0)]\ .$$

The last term in this expression gives only a contribution to the static dipole moment which does not interest us here, while the first and second terms give a contribution to the induced dipole moment of the form

$$P_2(\omega)=B\delta(\omega-2\omega_0)+B^*\delta(\omega+2\omega_0)\ , \tag{43}$$

or

$$P_2(t)=Be^{-i2\omega_0 t}+\text{c.c.}\ , \tag{44}$$

where

$$B=A(2\omega_0,\omega_0)E_0^2\ . \tag{45}$$

The radiation from this oscillating dipole gives rise to the SHG signal. If we have an ordered lattice of adsorbed alkali-metal atoms, we must sum up the scattered radiation from each dipole (plus its image in the substrate) in order to get the total SHG signal from the adsorbates.

Let us now discuss the magnitude and frequency dependence of the SHG signal. It is convenient to normalize the SHG signal for an adsorbate-covered surface to that of the clean surface. The second-order contribution to the normal dipole moment per unit area of a clean metal surface is conveniently written (at low frequencies)[18]

$$\frac{dP_2^{\text{clean}}}{dA}=\frac{a|E_0|^2}{64\pi^2 e n_{\text{bulk}}}\ , \tag{46}$$

where n_{bulk} is the number of free carriers per unit volume

in the bulk and a is a dimensionless, frequency-dependent and, in general, a complex valued function of the laser frequency ω. For the small frequencies which interest us here ($\hbar\omega \sim 1$ eV), experimental data indicate that for silver $a \approx -10$.

Consider now a metal surface with adsorbed alkali-metal atoms and let n denote the number of adsorbates per unit area. Including the dipole-dipole interaction between the adsorbates, we obtain from (44) and (45)

$$\frac{dP_2^{\text{ads}}}{dA} = \frac{nA(2\omega,\omega)|E_0|^2}{[1+\alpha(\omega)U]^2[1+\alpha(2\omega)U]} . \tag{47}$$

Hence we can write

$$\eta = \frac{dP_2^{\text{ads}}/dA}{dP_2^{\text{clean}}/dA} = -n\left[\frac{2e^2}{\Gamma_s}\right]^2 \frac{d^3 n_{\text{bulk}}}{a} \frac{Q(\omega)}{[1+\alpha(\omega)U]^2[1+\alpha(2\omega)U]} , \tag{48}$$

where

$$Q(\omega) = -16\pi^2 A(2\omega,\omega)\Gamma_s^2/(ed)^3 . \tag{49}$$

In Fig. 10, $|Q|$ is plotted as a function of the laser frequency ω and for several different alkali-metal coverages. Figure 11 shows the phase of Q [$Q = |Q| \exp(i\phi)$]. These calculations have been done using the same parameter values as before, namely $\varepsilon_s - \varepsilon_F = 2.4$ eV, $\Gamma_s = \Gamma_p = 1$ eV, $d = 1.9$ Å, $\lambda = 1.41$ Å, and $\varepsilon_p - \varepsilon_s = 1.6$ eV.

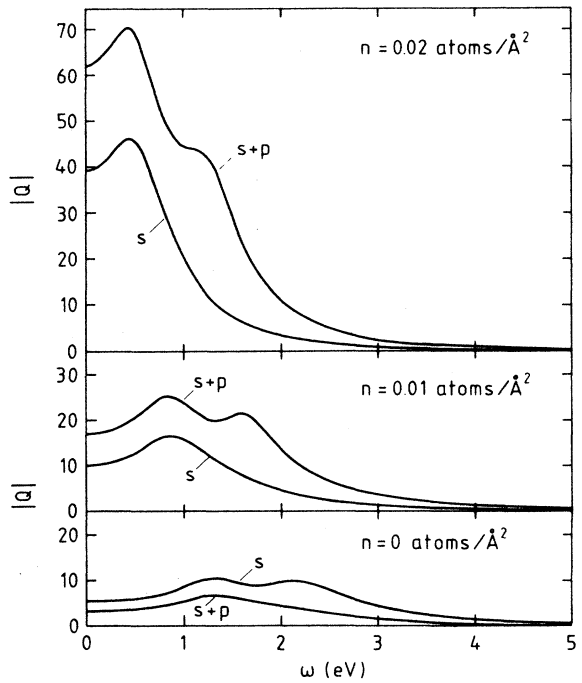

FIG. 10. The absolute magnitude of the function Q, which is proportional to the second-order induced dipole moment, is shown as a function of frequency and for several different alkali-metal coverages. The contribution from $s \rightarrow s$ transitions alone is shown separately. The same model parameters as in Fig. 1 are used.

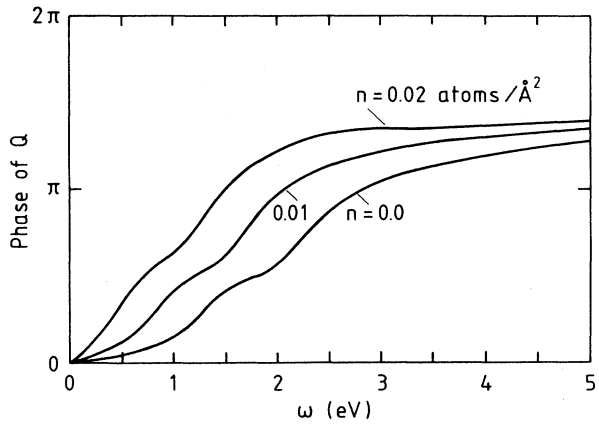

FIG. 11. The phase of Q.

A knowledge of the phase ϕ is important if several (approximately) independent processes contribute to the SHG signal. This is the case for low adsorbate coverages where the total second-order dipole moment per unit area is the sum of the contribution from the adsorbates plus the contribution from the clean surface, i.e.,

$$dP_2^{\text{tot}}/dA \approx dP_2^{\text{ads}}/dA + dP_2^{\text{clean}}/dA .$$

Depending on the relative phase between these two contributions, constructive or destructive interference will occur.[19]

The alkali-metal-induced enhancement of the SHG signal, $|\eta|^2$, is shown in Fig. 12 as a function of the alkali-metal coverage n and for the incident photon energy $\omega = 1.16$ eV. The fast decay of the SHG signal for $n \geq 0.02$ Å^{-2} is due to the strong (linear) screening of the electric field at the surface. This screening gives rise to the factor $[1+\alpha(\omega)U]^{-2}[1+\alpha(2\omega)U]^{-1}$ in (47) and gives a reduction in the SHG signal by a factor ≈ 0.03 at the alkali-metal coverage $n = 0.02$ Å^{-2} and by $\approx 2\times 10^{-4}$ at $n = 0.04$ Å^{-2} (see Fig. 7). Without this screening, $|\eta|^2$ would increase monotonically with increasing alkali-metal coverage n. It should be pointed out, however, that the present model calculation, which neglects the direct overlap in the wave functions of the alkali-metal atoms, is strictly valid only at relatively low alkali-metal coverage (perhaps $n \leq 0.02$ Å^{-2}). Nevertheless, recent model calculations by Liebsch,[20] which use a jellium slab on top of a semi-infinite jellium background to describe the alkali-metal-adsorbate system (this might be a reasonable model for *thick* alkali-metal layers), predict very small enhancements in the SHG signal. This is consistent with the strong (linear) screening (at $\hbar\omega = 1.16$ eV) in such systems. Hence it is very puzzling that the observed SHG signal increases monotonically up to about one monolayer alkali-metal coverage and then only very slowly decays in an oscillatory fashion with increasing film thickness (see Fig. 13). On the contrary, electron emission caused by two-photon absorption (which is possible

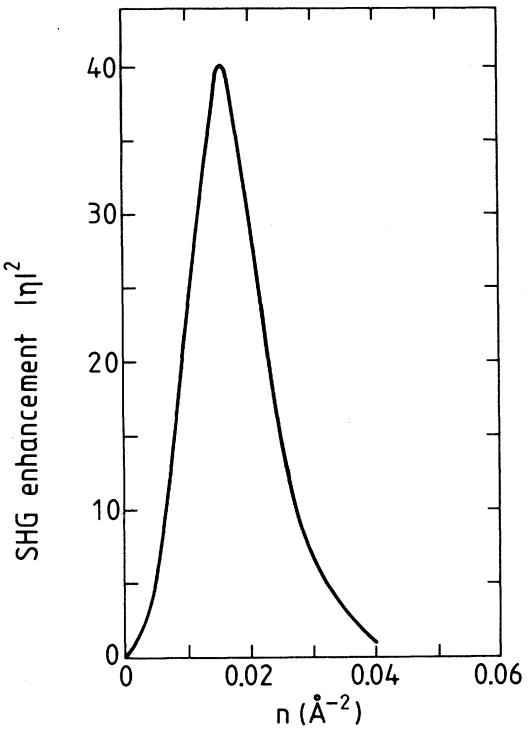

FIG. 12. The SHG enhancement as a function of the alkali-metal coverage n.

only when the alkali-metal coverage is so large that the work function $\phi < 2\hbar\omega \approx 2.32$ eV) does indeed show a peak centered at about $\frac{1}{2}$ monolayer for Rb on Ag(110) (see Fig. 13). The fast decay in the electron current for $n \geq \frac{1}{2}$ monolayer is almost certainly due to the strong (linear) screening of the external driving field (see below). The puzzling question is why this screening shows up in this case but not in the SHG data. However, one should note that while in linear optics light scattering and electron emission (the photoelectric effect) are both related to the (linear) polarizability [light scattering $\sim|\alpha(\omega)|^2$ while optical absorption $\sim \mathrm{Im}\alpha(\omega)$] such a simple and direct relation does not exist between SHG and electron emission caused by two-photon absorption. Indeed, the rate of electron emission is given by

$$w = \frac{2\pi}{\hbar} \sum_f \left| \left\langle f \left| \hat{\mu}\cdot E \frac{1}{H_0 - E_i - i0} \hat{\mu}\cdot E \right| i \right\rangle \right|^2 \delta(E_f - E_i) , \tag{50}$$

where the sum is over all final states $|f\rangle$ where two photons have been absorbed and one electron has been excited from an occupied level to an empty level corresponding to an electron which is leaving the adsorbate system. Hence the electron emission current is proportional to μ^4 while the SHG response function $\chi \sim \mu^3$ [see Eq. (33)] and no simple relation exists between the two processes.

The electric field E in (50) is the screened linear electric field, i.e., it contains the screening factor $[1+\alpha(\omega)U]^{-1}$ which therefore occurs to the fourth power in w and hence strongly reduces the photocurrent at "high" adsorbate coverage in agreement with the experimental data in Fig. 13.

Let us now discuss the magnitude of the SHG signal and its dependence on the laser frequency. At 1.16 eV photon energy, an enhancement of ~ 40 is found at $n \sim 0.015$ Å^{-2} (see Fig. 12). A strong increase in the SHG signal at low alkali-metal coverage is in accordance with the experimental data of Tom *et al.* and of Song *et al.* (see Fig. 13). The result presented in Fig. 12 has been calculated using $a = -10$. There exists at present some uncertainty about the actual magnitude of the a parameter for Ag at $\hbar\omega = 1.16$ eV. While some "old" experimental data[21] indicated $a \approx -1$ for Ag at $\hbar\omega = 1.16$ eV, there are new experimental data by Song and Plummer which suggest $a \approx -10$. This is consistent with the theoretical work of Weber and Liebsch[22] and of Chizmeshya and Zaremba[23] using the jellium model described earlier and treating the electron-electron interaction within the density-functional scheme in the local-density approximation (LDA) (Weber and Liebsch) or in the hydrodynamic approximation (Chizmeshya and Zaremba). However, the LDA is known to overestimate the nonlinear response of atoms by typically a factor of 2 and the same might be true for metal surfaces. In addition, the jellium model does not account for the d bands in the noble and transition metals and does not give the correct work function. All of these factors taken together make a theoretical estimate of the a parameter very uncertain for both transition and noble metals. It is unlikely that this fact will change the qualitative result that

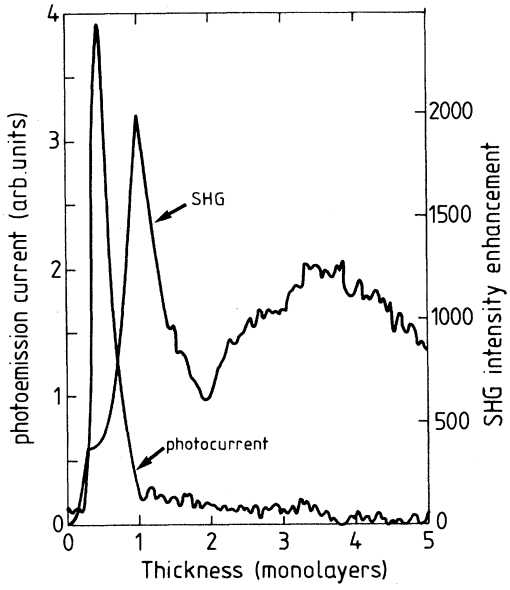

FIG. 13. The SHG signal [normalized to that of the clean Ag(110) surface] and the electron emission current as a function of the alkali-metal thickness (in monolayers). The experimental data are for Rb on Ag(110) and are obtained by Song *et al.* (Ref. 5).

the model studied in this work gives a strong enhancement in the SHG at low alkali-metal coverage.

Finally, concerning the frequency dependence of the SHG signal, it is obvious from Fig. 10 that as the laser frequency is doubled (from 1.16 to 2.32 eV), $|Q|$ decreases and this leads to a decreased SHG signal in qualitative agreement with the experimental data.[4,5]

VI. TEMPERATURE-DEPENDENT LOCAL FIELDS

Alkali-metal atoms adsorbed on noble or transition metals at low coverages are largely ionized. The resulting strong repulsive interaction between the alkali-metal atoms makes them form (almost) ordered lattice structures if the temperature is low enough.[24] For ordered structures the local electric fields E_i and the induced dipole moments p_i are identical for all of the adsorbates and are related via $E=-Up$ where the dipole sum U can be written

$$U=\sum_i \frac{2}{|\mathbf{x}_i|^3}\approx 18\Theta^{3/2}/a^3 . \tag{51}$$

Here the factor of 2 accounts for image dipoles and a is the lattice constant (assuming a simple square lattice) associated with the alkali-metal-monolayer surface unit cell and Θ is the corresponding alkali-metal coverage. As the temperature is raised, the adsorbate lattice will start to disorder. For example, at low alkali-metal coverage it is known that the alkali-metal-induced low-energy electron diffraction rings typically disappear at ~ 300 K. As a result, the dipole sum in (51) is no longer over a regular lattice and the local electric fields E_i and the induced dipole moments p_i are no longer identical for all of the adsorbates. In the limiting case of complete disorder, where the adsorbates are distributed randomly (but with an average concentration $n=\Theta/a^2$) over the substrate binding sites, the dipole sum becomes $U(\text{random})\approx 18\Theta/a^3$. This differs by a factor $\Theta^{1/2}$ from U (ordered) and at low alkali-metal coverage (say $\Theta\sim 0.01$) this is a very large "correction." In practice it is impossible to reach the limit of complete disorder by simply increasing the temperature (it would require such a high temperature that the alkali-metal atoms desorb almost instantaneously), but the argument indicates that non-negligible temperature-dependent changes in the local fields E_i and dipole moments p_i may occur as the temperature is raised. In this section, we will discuss this problem in some detail.

Consider first the idealized case where the substrate is perfectly smooth (i.e., the alkali-metal binding energy is the same everywhere within the surface unit cell). In this case, the alkali-metal atoms would form (at zero temperature) a perfectly ordered (triangular) lattice structure. However, a real surface is corrugated with one site within each surface unit cell having a higher binding energy than the other sites. At low alkali-metal coverage, the state of highest binding energy is obtained by displacing the alkali-metal atoms slightly away from their ideal lattice positions to the nearest site of high binding energy. This results in disorder. In the discussion which follows we will only focus on the very low coverage case here, for our purposes, this weak disorder can be neglected. Hence, when calculating the spatial distribution of adsorbates at thermal equilibrium, we can treat the substrate as perfectly smooth and assume that the adsorbates (at zero temperature) form a regular lattice structure.

Suppose that we increase the surface temperature. Due to thermal motion, the alkali-metal atoms will now temporarily occupy binding sites away from the lattice sites occupied at zero temperature. Let us calculate the total lateral interaction energy after the alkali-metal atoms have been displaced by vectors $\mathbf{b}_i$ $(i=1,\ldots,N)$, $\mathbf{x}_i\rightarrow\mathbf{x}_i+\mathbf{b}_i$:

$$E(b)=\tfrac{1}{2}\sum_{ij}{}' \frac{2p_ip_j}{|\mathbf{x}_i+\mathbf{b}_i-\mathbf{x}_j-\mathbf{b}_j|^3} , \tag{52}$$

where the factor of 2 accounts for image dipoles. For the ordered lattice ($T=0$) all the alkali-metal atoms give rise to the same dipole moment because the local electric field at each alkali-metal atom from the dipoles associated with all the other alkali-metal atoms is identical. However, for $T\neq 0$, we will have a distribution of induced dipoles. The dipole moment p_i of adsorbate i is a function of the local electric field E_i. At low alkali-metal coverage, where E_i is small, we can expand

$$p_i=p(E_i)\approx p(0)+\alpha E_i , \tag{53}$$

where $\alpha=dp/dE$ at $E=0$. Note that both $p(0)$ and α can be calculated from the dependence of the work function on the alkali-metal coverage at low temperature (see below).

Expanding the interaction energy $E(b)$ to second order in $\mathbf{b}_i$ gives

$$E(b)=E(0)+E_{\alpha\beta}b_\alpha b_\beta , \tag{54}$$

where we have introduced the "state" vector b_β with $2N$ components [the x and y components of $\mathbf{b}_i$ $(i=1,\ldots,N)$] and where summation over repeated indices (α,β) is implicitly understood. There is no linear term in the expansion (54) since $b_\beta=0$ is a minimum of $E(b)$. Next we expand p_i to second order in b:

$$p_i=p(n)+p_{i\alpha}b_\alpha+p_{i\alpha\beta}b_\alpha b_\beta , \tag{55}$$

where $p(n)$ is the dipole moment of an adsorbate when $b_\alpha=0$ and at the alkali-metal coverage n under consideration. Now, since

$$E_i=-\sum_j{}' U_{ij}p_j , \tag{56}$$

where

$$U_{ij}=\frac{2}{|\mathbf{x}_i+\mathbf{b}_i-\mathbf{x}_j-\mathbf{b}_j|^3} , \tag{57}$$

we get from (53) and (56)

$$p_i = p(0) - \alpha \sum_j{}' U_{ij} p_j \ . \tag{58}$$

Next, we multiply this equation by p_i and sum over i to get

$$\sum_i p_i^2 = p(0) \sum_i p_i - 2\alpha E(b) \ . \tag{59}$$

Substituting (54) and (55) in (59) gives, to second order in b_α,

$$Np^2(n) + 2\sum_i p(n) p_{i\alpha} b_\alpha + \sum_{i,j} p_{i\alpha} p_{j\beta} b_\alpha b_\beta + 2p(n) \sum_i p_{i\alpha\beta} b_\alpha b_\beta$$
$$= Np(0)p(n) + p(0) \sum_i p_{i\alpha} b_\alpha + p(0) \sum_i p_{i\alpha\beta} b_\alpha b_\beta - 2\alpha [E(0) + E_{\alpha\beta} b_\alpha b_\beta] \ .$$

Since b_α is arbitrary, we get

$$Np^2(n) = Np(0)p(n) - 2\alpha E(0) \ , \tag{60}$$

$$[2p(n) - p(0)] \sum_i p_{i\alpha} = 0 \ , \tag{61}$$

$$\sum_{ij} p_{i\alpha} p_{i\beta} + [2p(n) - p(0)] \sum_i p_{i\alpha\beta} = -2\alpha E_{\alpha\beta} \ . \tag{62}$$

Since, in general, $2p(n) \neq p(0)$, (61) gives

$$\sum_i p_{i\alpha} = 0 \tag{63}$$

and (62) reduces to

$$\sum_i p_{i\alpha\beta} = -\frac{\alpha}{p(n) - p(0)/2} E_{\alpha\beta} \ . \tag{64}$$

Using (55), (63), and (64) gives

$$\sum_i p_i = Np(n) - \frac{\alpha}{p(n) - p(0)/2} E_{\alpha\beta} b_\alpha b_\beta$$

or

$$\langle p_i \rangle = \frac{1}{N} \sum_i p_i = p(n) - \frac{\alpha}{p(n) - p(0)/2} \frac{1}{N} \langle E(b) - E(0) \rangle$$
$$= p(n) - \frac{\alpha}{p(n) - p(0)/2} k_B T \ . \tag{65}$$

Using (53), we get

$$\langle p_i \rangle = p(0) + \alpha \langle E_i \rangle$$

and combining this with (65), we obtain

$$\langle E_i \rangle = \frac{p(n) - p(0)}{\alpha} - \frac{k_B T}{p(n) - p(0)/2} \ . \tag{66}$$

To determine α, let us consider an ordered lattice of adsorbates (i.e., $T = 0$), where

$$E = -Up \ .$$

Furthermore, in this case (53) takes the form

$$p(n) = p(0) + \alpha E$$
$$= p(0) - \alpha U p(n) \ .$$

Hence

$$\alpha = \frac{p(0) - p(n)}{Up(n)} \ .$$

Substituting this in (65) and (66) gives the final results

$$\langle p_i \rangle = p(n) - \frac{p(0) - p(n)}{Up(n)[p(n) - p(0)/2]} k_B T \ , \tag{67}$$

$$\langle E_i \rangle = -Up(n) - \frac{k_B T}{p(n) - p(0)/2} \ , \tag{68}$$

and the work-function change

$$\Delta\phi = 4\pi n e \langle p_i \rangle$$
$$= \Delta\phi_0(n) - 4\pi n e \frac{p(0) - p(n)}{Up(n)[p(n) - p(0)/2]} k_B T \ , \tag{69}$$

where $\Delta\phi_0(n)$ is the work function at low temperature. Note that this level of theory is only valid when the alkali-metal coverage is small and one is well away from any singularity in Eqs. (64)–(69). These formulas can be used to estimate the temperature dependence of the average local field $\langle E_i \rangle$ and of the work function. For example, for K on Cu(100) we get, at the coverage $n = 0.01$ Å^{-2}, a 20% increase in the local field $\langle E_i \rangle$ and a 4% decrease (≈ 120 meV) in the work-function lowering, as the temperature increased from 0 to 600 K. The temperature dependence of the work function of a clean metal surface is typically ten times weaker than for an alkali-metal-covered surface [e.g., for a clean Pt(111) surface ϕ decreases by about 15 meV as the temperature is raised from 0 to 600 K (Ref. 25)].

We have performed work-function measurements to test these theoretical predictions.[26] For a clean Cu(100) surface the work function decreases by 8 ± 2 meV when the surface temperature increases from 100 to 500 K. At the K coverage $n = 0.009$ Å^{-2} the work function increases by 41 ± 11 meV as the temperature increases from 100 to 420 K. Assuming that the work-function change of the clean surface and of the alkali-metal-covered surface are additive this gives a net $\approx 50 \pm 10$ meV alkali-metal-induced increase in the work function. This is in reasonably good agreement with the theoretical prediction, 65 meV, according to Eq. (69) and Fig. 1.

VII. SUMMARY AND CONCLUSION

In this work, we have developed a simple but realistic model for alkali-metal absorption on metal surfaces. The

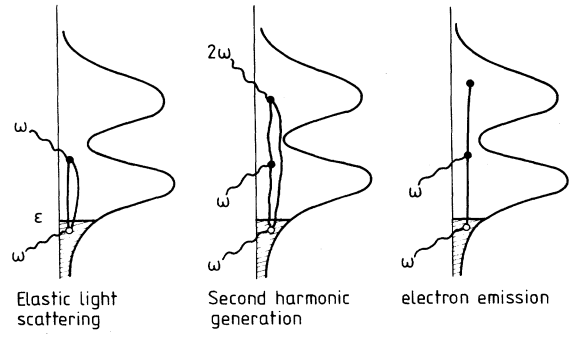

FIG. 14. A schematic representation of three processes discussed in this work.

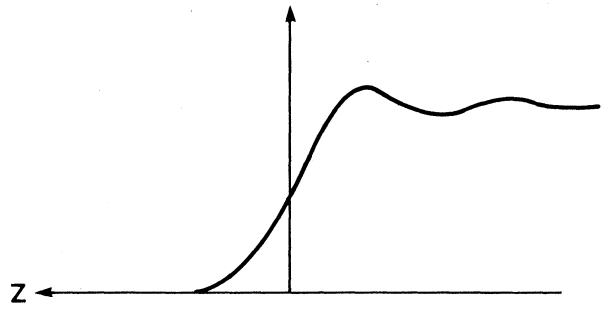

FIG. 15. The electron density profile at a surface.

influence of a low concentration of adsorbed alkali-metal atoms on (a) the work function; (b) the surface polarizability; and (c) the SHG signal has been analyzed in detail (see Fig. 14). The same model with the same model parameters was used in all of our calculations. The surface polarizability and SHG signal are determined by the first- and second-order (in the external driving field) induced dipole moments and these quantities were calculated using standard linear and quadratic response theory. The main results of the analysis are the following.

(a) The alkali-metal-induced peaks observed in the electron-energy-loss spectra at low alkali-metal coverage are the result of electronic transitions from the filled part of the *ns* resonance to the unoccupied part of the same resonance and to the *np* resonance. In addition, the surface becomes much more "lossy" at low frequencies.

(b) The model predicts a strongly enhanced SHG signal at low alkali-metal coverage (at the photon energy $\hbar\omega = 1.16$ eV). At higher alkali-metal coverage the SHG signal is predicted to decrease due to screening; this is not in accordance with the experimental data which show a monotonic increase in the SHG signal up to full monolayer coverage. We have no explanation for this puzzling discrepancy between theory and experiment.

(c) The temperature dependence of the work function is quite small, typically of order 5% as the temperature increases from 0 to 600 K.

ACKNOWLEDGMENTS

We thank K. J. Song for useful correspondence and N. D. Lang, A. Liebsch, and E. W. Plummer for useful discussions.

APPENDIX A

Here we will prove Eq. (14). In so doing, we will first consider a more general problem (which has been treated earlier in the literature;[27] however, the proof given below is simpler). Consider a semi-infinite medium with a surface electron density profile which varies in space as illustrated in Fig. 15. For a clean metal surface, for example, this spatial variation would arise from the electronic wave functions which decay into the vacuum. We want to calculate the response of this system to an external time-varying electric potential of the form

$$\phi_{\text{ext}} = \frac{2\pi}{q_\parallel} e^{i(\mathbf{q}_\parallel \cdot \mathbf{x}_\parallel - \omega t)} e^{q_\parallel z} ,$$

where the prefactor $2\pi/q_\parallel$ has been chosen for later convenience. If the medium can be treated as translationally invariant parallel to the surface, then the total potential outside the medium must have the form

$$\phi_> = \frac{2\pi}{q_\parallel} e^{i(\mathbf{q}_\parallel \cdot \mathbf{x}_\parallel - \omega t)} (e^{q_\parallel z} - g e^{-q_\parallel z}) , \tag{A1}$$

where the linear response function g depends on $q_\parallel$ and ω. The external potential ϕ_{ext} will induce a charge distribution ρ_{ind} which we assume is localized within a slab at the surface. Outside this slab, the potential which ρ_{ind} gives rise to can be represented as a multipole expansion, i.e., we formally replace the continuous charge density ρ_{ind} by the multipole expansion (including only the first two multipoles)

$$[\sigma\delta(z) + p\delta'(z)] e^{i(\mathbf{q}_\parallel \cdot \mathbf{x}_\parallel - \omega t)} ,$$

where σ and p are the charge and dipole moment per unit surface area, i.e.,

$$\sigma = \int dz\, \rho_{\text{ind}} ,$$

$$p = \int dz\, z \rho_{\text{ind}} .$$

In the multipole expansion we have only kept the first two moments. Next we use

$$\delta(z) = \frac{1}{2\pi} \int dk\, e^{ikz}$$

so that the multiple expansion of the induced charge density takes the form

$$\frac{1}{2\pi} \int dk\, (\sigma + ikp) e^{ikz} e^{i(\mathbf{q}_\parallel \cdot \mathbf{x}_\parallel - \omega t)} .$$

Substituting this into Poisson's equation

$$\nabla^2 \phi_{\text{ind}} = -4\pi \rho_{\text{ind}}$$

gives

$$\phi_{\text{ind}} = 2 \int dk \frac{e^{ikz}}{k^2 + q_\parallel^2} (\sigma + ikp) e^{i(\mathbf{q}_\parallel \cdot \mathbf{x}_\parallel - \omega t)}$$

$$= \frac{2\pi}{q_\parallel} (\sigma \pm q_\parallel p) e^{-q_\parallel |z|} e^{i(\mathbf{q}_\parallel \cdot \mathbf{x}_\parallel - \omega t)} ,$$

where $\pm$ refers to $z>0$ and $z<0$. The total potential is the sum of the external plus induced potential, i.e.,

$$\phi=\frac{2\pi}{q_\parallel}e^{(i\mathbf{q}_\parallel\cdot\mathbf{x}_\parallel-\omega t)}[e^{q_\parallel z}+(\sigma\pm q_\parallel p)e^{-q_\parallel|z|}] . \tag{A2}$$

Now, since in general σ depends on $q_\parallel$ we get for small $q_\parallel$

$$\sigma\approx\sigma_0+q_\parallel\sigma_1 ,$$

where σ_0 and σ_1 depend only on ω. Substituting this into (A2) and making use of the standard boundary condition

$$\left.\frac{\partial\phi}{\partial z}\right|_{0^+}-\epsilon\left.\frac{\partial\phi}{\partial z}\right|_{0^-}=0 , \tag{A3}$$

gives

$$1-\sigma_0-(\sigma_1+p)q_\parallel-\epsilon[1+\sigma_0+(\sigma_1-p)q_\parallel]=0 .$$

This equation should be valid for all (small) $q_\parallel$, i.e.,

$$\sigma_0=\frac{1-\epsilon}{1+\epsilon} ,$$

$$\sigma_1=-\sigma_0 p .$$

Using these two equations, for $z>0$ the term in parentheses in (A2) becomes

$$e^{q_\parallel z}-\frac{\epsilon-1}{\epsilon+1}\left[1+\frac{2\epsilon}{\epsilon+1}\frac{p}{\sigma_0}q_\parallel\right]e^{-q_\parallel z} .$$

Comparing this with (A1) gives

$$g(\mathbf{q}_\parallel,\omega)=\frac{\epsilon-1}{\epsilon+1}\left[1+\frac{2\epsilon}{\epsilon+1}d_\perp(\omega)q_\parallel\right] , \tag{A4}$$

where

$$d_\perp=\frac{p}{\sigma_0}=\frac{\int dz\, z\rho_{\rm ind}}{\int dz\,\rho_{\rm ind}} \tag{A5}$$

is the centroid of the induced charge density for $q_\parallel=0$. The proof of (A4) results from a systematic expansion of all quantities to first order in $q_\parallel$, except for the boundary condition (A3) which is valid only to zero order in $q_\parallel$. However, one can generalize this boundary condition to finite $q_\parallel$ but one finds that the extra term linear in $q_\parallel$ vanishes identically if the origin $z=0$ is suitably chosen.

Let us now apply the general result (A4) to the case of adsorbed atoms. Let us assume that the atoms can be treated as point particles with polarizability $\alpha(\omega)$ and that the particles occupy the sites of a regular lattice. We then have

$$p=\alpha E_{\rm loc} ,$$

$$\sigma_0=\frac{1-\epsilon}{1+\epsilon} ,$$

where $E_{\rm loc}$ is the local electric field at an adsorbate. The external electric field is obtained from (A1)

$$E_{\rm ext}=-\frac{\partial\phi_{\rm ext}}{\partial z}=-2\pi \quad \text{as } q_\parallel\to 0 .$$

The dipole moment p can be written

$$p=\alpha E_{\rm loc}=\alpha\left[\frac{2\epsilon}{\epsilon+1}E_{\rm ext}-U_0 p-\frac{\epsilon-1}{\epsilon+1}U_0 p\right] ,$$

where

$$U_0=\sum_i{}' \frac{1}{|\mathbf{x}_i|^3} .$$

The equation above can be solved for p to give

$$p=\frac{\alpha}{(\epsilon+1)/2\epsilon+\alpha U_0}E_{\rm ext}$$

and

$$d_\perp=\frac{pn}{\sigma_0}=2\pi\frac{\epsilon+1}{\epsilon-1}\frac{n\alpha}{(\epsilon+1)/2\epsilon+\alpha U_0} .$$

Substituting this into (A4) gives

$$g=\frac{\epsilon-1}{\epsilon+1}+4\pi\frac{\epsilon}{\epsilon+1}\frac{n\alpha q_\parallel}{(\epsilon+1)/2\epsilon+\alpha U_0} .$$

We only focus on low frequencies ($\omega\ll\omega_p$) where $|\epsilon|\gg 1$. Hence we can take $\epsilon\to\infty$ in the last term in g to get

$$g=\frac{\epsilon-1}{\epsilon+1}+8\pi\frac{n\alpha q_\parallel}{1+\alpha U} ,$$

where $U=2U_0$. Hence we have proved Eq. (14).

APPENDIX B

Since

$$\rho_{ab}(\varepsilon)=\langle a|\delta(\varepsilon-H_0)|b\rangle ,$$

$$\rho_a(\varepsilon)=\langle a|\delta(\varepsilon-H_0)|a\rangle ,$$

and similarly for $\rho_b(\varepsilon)$, it follows from a generalized Schwartz inequality that

$$\rho_{ab}(\varepsilon)\le[\rho_a(\varepsilon)\rho_b(\varepsilon)]^{1/2} .$$

Hence, if the resonances ρ_a and ρ_b have negligible overlap, then $\rho_{ab}\approx 0$. Note also that while

$$\int_{-\infty}^{\infty}d\varepsilon\,\rho_a=1$$

we have

$$\int_{-\infty}^{\infty}d\varepsilon\,\rho_{ab}=0 .$$

The quantity $\rho_{ab}(\varepsilon)$ contains information about the extent that orbitals $|a\rangle$ and $|b\rangle$ can "communicate" via the metal conduction band $\{|k\rangle\}$, to which they both are connected via the hybridization interactions V_{ak} and V_{bk}. The quantity ρ_{ab} is important when studying the indirect (via the metal conduction band) static or dynamic interaction between molecules adsorbed on a metal surface. In this case, $|a\rangle$ and $|b\rangle$ could be the same type of orbitals in two identical molecules separated laterally by a vector $\mathbf{R}$ (see Ref. 28 for details on this class of problems).

[1]For an extensive review, see H. P. Bonzel, Surf. Sci. Rep. **8**, 43 (1987), and references therein.
[2]See, for example, S. Andersson and U. Jostell, Surf. Sci. **46**, 625 (1974); S. Å. Lindgren and L. Waldén, Phys. Rev. B **22**, 5967 (1980).
[3]D. Hesket, K. H. Frank, E. E. Koch, and H. J. Freund (unpublished).
[4]H. W. K. Tom, C. M. Mate, X. D. Zhu, J. E. Crowell, Y. T. Shen, and G. A. Somorjai, Surf. Sci. **172**, 466 (1986).
[5]K. J. Song, D. Hesket, E. W. Plummer, and H. L. Dai (unpublished).
[6]B. Woratschek, W. Sesselmann, J. Küppers, G. Ertl, and H. Haberland, Phys. Rev. Lett. **55**, 1231 (1985).
[7]J. P. Muscat and D. M. Newns, J. Phys. C **7**, 2630 (1974).
[8]N. D. Lang and A. R. Williams, Phys. Rev. B **18**, 616 (1977); N. D. Lang (private communication).
[9]L. H. Dubois, B. R. Zegarski, and H. S. Luftman, J. Chem. Phys. **87**, 1367 (1987).
[10]N. D. Lang and W. Kohn, Phys. Rev. B **7**, 33 541 (1973).
[11]J. P. Muscat and I. P. Batra, Phys. Rev. B **34**, 2889 (1986).
[12]B. N. J. Persson and J. E. Demuth, Phys. Rev. B **30**, 5968 (1984).
[13](a) S. Andersson and B. N. J. Persson, Phys. Rev. Lett. **50**, 2028 (1983); (b) B. N. J. Persson and E. Zaremba, Phys. Rev. B **31**, 1863 (1985).
[14]A. G. Eguiluz and D. A. Campbell, Phys. Rev. B **31**, 1512 (1985).
[15]C. K. Chen, T. F. Heinz, D. Ricard, and Y. R. Shen, Phys. Rev. Lett. **46**, 1010 (1981); H. W. K. Tom, T. F. Heinz, and Y. R. Shen, *ibid.* **51**, 1983 (1985).
[16]T. F. Heinz, M. M. T. Loy, and W. A. Thompson, Phys. Rev. Lett. **54**, 63 (1985).
[17]H. W. K. Tom, C. M. Mate, X. D. Zhu, J. E. Crowell, T. F. Heinz, G. A. Somorjai, and Y. R. Shen, Phys. Rev. Lett. **52**, 348 (1984).
[18]J. Rudnick and E. A. Stern, Phys. Rev. B **4**, 4274 (1971).
[19]W. Heuer, L. Schröter, and H. Zaccharias, Chem. Phys. Lett. **135**, 299 (1987).
[20]A. Liebsch (unpublished).
[21]J. C. Quail and H. J. Simon, Phys. Rev. B **31**, 4900 (1985).
[22]M. Weber and A. Liebsch, Phys. Rev. B **35**, 7411 (1987); see also M. Corri and W. L. Schaich, *ibid.* **33**, 3688 (1986).
[23]A. Chizmeshya and E. Zaremba, Phys. Rev. B **37**, 2805 (1988).
[24]R. L. Gerlach and T. N. Rhodin, Surf. Sci. **17**, 32 (1969); **19**, 403 (1970).
[25]G. Ertl, M. Neumann, and K. M. Streit, Surf. Sci. **64**, 393 (1977).
[26]All $\Delta\phi$ measurements were performed using the ac retarding potential technique; R. Nathan and B. J. Hopkins, J. Phys. E **7**, 851 (1974).
[27]P. J. Feibelman, Prog. Surf. Sci. **12**, 287 (1982).
[28]T. L. Einstein and J. R. Schrieffer, Phys. Rev. B **7**, 3629 (1973); T. B. Grimley, Proc. Phys. Soc. London **90**, 751 (1967); B. N. J. Persson, Surf. Sci. **116**, 585 (1982).